Selective microwave sensors exploiting the interaction of analytes with trap states in TiO_2 nanotube arrays†

M. H. Zarifi,[1] S. Farsinezhad,[1] M. Abdolrazzaghi,[1] M. Daneshmand[1] and K. Shankar[1, 2]

[1]*Department of Electrical and Computer Engineering, University of Alberta, Edmonton, Alberta, T6G 2V4, Canada*

[2]*National Institute for Nanotechnology, National Research Council, Edmonton, Alberta, T6G 2M9, Canada*

Abstract

Sensing of molecular analytes by probing the effects of their interaction with microwaves is emerging as a cheap, compact, label-free and highly sensitive detection and quantification technique. Microstrip ring-type resonators are particularly favored for this purpose due to their planar sensing geometry, electromagnetic field enhancements in the coupling gap and compatibility with established printed circuit board manufacturing. However, the lack of selectivity in what is essentially a permittivity-sensing method, is an impediment to wider adoption and implementation of this sensing platform. By placing a polycrystalline anatase-phase TiO_2 nanotube membrane in the coupling gap of a microwave resonator, we engineer selectivity for the detection and differentiation of methanol, ethanol and 2-propanol. The scavenging of reactive trapped holes by aliphatic alcohols adsorbed on TiO_2 is responsible for the alcohol-specific detection while the different short chain alcohols are distinguished on the basis of differences in their microwave response. Electrodeless microwave sensors which allow spectral and time-dependent monitoring of the resonance frequency and quality factor provide a wealth of information in comparison to electrode-based resistive sensors for the detection of volatile organic compounds. A high dynamic range (400 ppm - 10000 ppm) is demonstrated for methanol detection.

KEYWORDS: Split ring resonators, microwave metamaterials, small molecule sensing, recombination, photodielectric effect, complex permittivity, deep traps, nanodielectrics.

† Electronic Supplementary Information (ESI) available. see DOI:

Microwave resonators have shown their capability as sensing devices in a wide range of applications not only for analytes in the solid and liquid phase, but also recently in a gaseous environment.[1-6] Planar microstrip resonators made from metamaterial-inspired split ring resonators (SRRs) have shown relatively sharper resonances and concomitantly increased sensitivity due to their higher coupling to the surrounding signal lines.[7-9] These sensors are amenable to miniaturization, automation, mass production and wireless interconnection due to CMOS compatibility, low cost and a facile fabrication process.[10] Such microwave resonators also offer noninvasive sensing through contact-less probing, which adds to their flexibility of usage and maneuverability for *in situ* characterization. Since SRR based passive sensors have a low response time and can almost instantly translate changes in the environment of study into measurement quantities, they can be used as real-time sensors.[11, 12]

The physical principle of all microwave sensors consists of the detection of the change in the complex permittivity of the active sensing region (coupling gap for a planar resonator or location of a resonant node for a cavity waveguide) due to the analyte. The concentration of the analyte is deduced from the changes induced in the complex permittivity. In gas sensing, when the vapor type or concentration changes, the total effective permittivity variation is very small and cannot be directly detected by microwave sensors. This has been partially addressed in prior reports by the use of reagent-intensive binding receptors on the surface[13] and/or incorporation of spectroscopic permittivity measurements.[14, 15] In addition, most microwave sensors are primarily permittivity detectors that are oblivious to chemical differences due to the permittivity being a rather blunt detection tool and further improvements in selectivity are needed before the advantages of microwave sensing can truly be brought to bear in applications such as gas sensing

in composite mixtures. Moreover, a key goal in the sensing field is the generation of selectivity without the use of immobilized chemoselective receptors.[16]

We propose the use of high-surface area semiconductor nanomaterials integrated into the active region of microwave resonators as a re-usable and selective sensing matrix. The selectivity is engineered through the detection by microwaves of the specific interactions of the analytes with trap states in the semiconductor. We demonstrate this concept using an open loop microstrip resonator containing a titania nanotube membrane in its coupling gap. Different low molecular weight alcohols are distinguished by microwaves on the basis of their interaction with reactive trapped photogenerated holes in the TiO_2 nanotubes and the resulting effect on the complex permittivity of the membrane.

Surface trap states in semiconductor thin films and nanostructures have generally been viewed negatively due to their deleterious effects on charge transport and luminescence in the active layers of switching, sensing, light emitting and light harvesting devices. This view underwent a change first in field effect transistor chemobiological sensors wherein the perturbation of the charge transport in the channel induced by surface adsorption of the analyte was exploited to increase sensitivity of detection.[17, 18] Likewise, nitrogen vacancy color centers in diamond have recently found use for the highly sensitive detection of magnetic fields, electric fields and temperature.[19, 20] Surface traps have also been used in a positive role to increase the sensitivity and tune the temporal response of photodetectors.[21, 22] Our study adds to the small but growing body of literature on the beneficial use of surface trap states by demonstrating the semiconductor surface trap-mediated engineering of selectivity in microwave sensing.

A planar open loop resonator with a resonance frequency of 5.12 GHz and a quality factor of 233 was designed and fabricated for use in sensing. The structure of the resonator is schematically illustrated in Fig. 1, parts a and b along with a presentation of the results of Finite Element Method (FEM) simulations of the resonator using HFSS software. The electric field distribution in a plane with a constant distance of 1 mm from the resonator's surface shows the hot-spots on that plane. These regions demonstrate more sensitivity to permittivity variation than the other regions in the close neighborhood of the resonator due to the capacitive mutual coupling between the split ring resonator and the transmission line. Fig. 1b shows the electric field distribution over the sensor at two distinct frequencies. The maximum power transmission in the microstrip transmission line structure occurs at the frequency at which the length of the SRR equals half the wavelength. Likewise, the maximum electric field concentration is observed at the resonance frequency in the coupling gap of the resonator and decreases precipitously as either the frequency is moved away from resonance or the spatial location is moved away from the coupling gap. Fig. 1c shows the surface current distribution at the resonant frequency and indicates a high concentration of surface currents in the whole area of SRR, illustrating the fundamental (first) resonance, as well as strong coupling between transmission line and SRR. Fig. 1d depicts the frequency response of the bare resonator, where there is no analyte over it. The scattering parameter S21 indicates the power of the transmitted microwave signal from the input to the output (in dB) while S11 measures the reflected power. Experimental details including, but not limited to, the resonator fabrication and measurement set-up, the monitoring of the environmental variables during the sensing tests, the preparation of the nanotube membrane sensing layer and the characterization of the nanotube membrane are provided in Section S1 in ESI†.

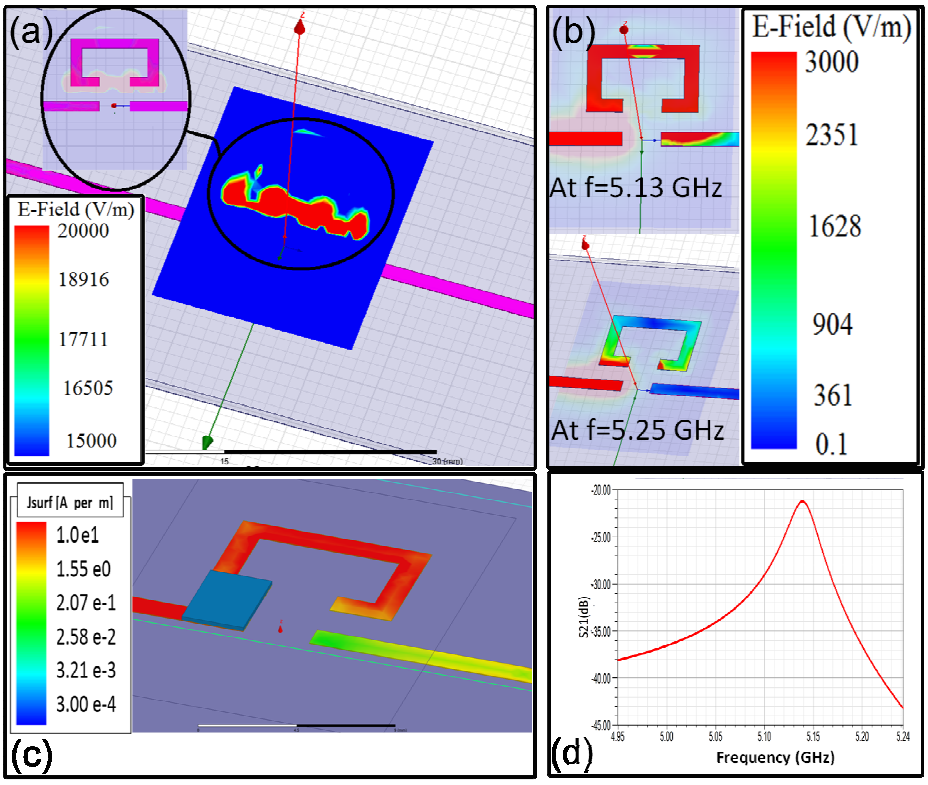

Fig. 1 (a) Electric field intensities on the resonator substrate, field distribution and hot spots are shown (b) Field propagation comparison at resonance and off-resonance (c) Surface current density distribution on the resonator surface and (d) S21 resonant profile of the resonator.

The presence of the TiO_2 nanotube membrane in the coupling gap (also the most sensitive region) of the resonator affects the resonator characteristics and creates a downshift in the resonance frequency of ~90 MHz (Fig. S1 in ESI†). The quality factor reduced from 233 to 75 due to the increased capacitive coupling between the signal line and the resonance strip line owing to the higher permittivity (in comparison to air and the substrate) of the TiO_2 nanotube membrane and also due to absorption of microwaves by electrons in *n*-TiO_2 nanotubes (Fig. S1 in ESI†) whose carrier concentration is known to be 10^{18}-10^{20} cm^{-3}.[23] Post-measurement simulations of the microwave response of the membrane in the coupling gap were performed using HFSS (Fig. 2) and matched with the experimental data to extract the complex microwave permittivity of the TiO_2 nanotube membrane. Using this method, the effective dielectric constant

and loss tangent of TiO_2 nanotubes at ~5 GHz were found to be 9.75 and 0.36 respectively (Fig. S1 in ESI†). As seen in Fig. 2, a 16 % variation of relative permittivity and 40 % variation in the loss tangent (tan δ) of the membrane produces a 12 MHz variation in the resonance frequency. These simulations describe the behavior of the nanotube membrane during photoexcitation and also during the subsequent relaxation period.

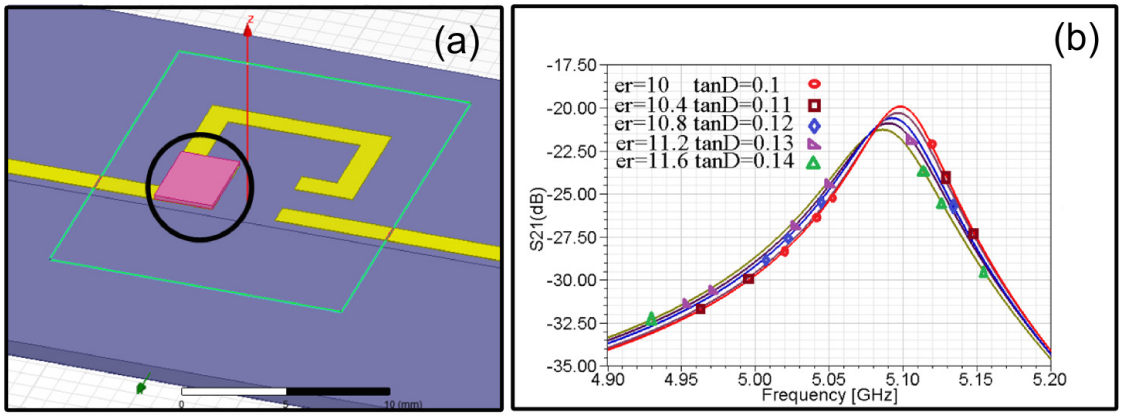

Fig. 2 (a) Schematic of the resonator with a nanotube membrane mounted on top of the resonator and (b) Simulation results showing the effect of permittivity and loss tangent variation in the nanotube membrane on the resonant profile.

A 254 nm ultraviolet (UV) curing lamp was used to illuminate the membrane for five minutes at room temperature and at an incident intensity of 0.5 mW cm^{-2}. The lamp was positioned far enough from the surface of the nanotube membrane and the illumination intensity was low enough so that membrane heating effects could be neglected. For each fresh membrane, two sets of experiments were performed (a) UV illumination without the presence of volatile organic compound (VOC) vapor and (b) UV illumination of the same membrane followed by introduction of VOC vapor after the stoppage of illumination. Fig. 3a shows the experiment setup and its schematics. During photoexcitation and the subsequent relaxation, variations in the amplitude, resonance frequency and quality factor of the resonance profile were observed. The forward transmission coefficient (S21) of the resonator during the illumination period is shown

in Fig. 3b. Fig. 3, parts c and d compare the behavior of the resonant frequency and quality factor during a time period of 5 hours for the membrane in air and for the membrane exposed to methanol vapor respectively. The inset in Fig. 3d is a magnified view of the absolute value of the Q factor as a function of time that clearly depicts the different phases that occur while the experiment runs and the turning points in the quality factor graph explicitly show sharp transitions prior to illumination (PI), during illumination (I), during relaxation(R) and during vapor exposure (VE).

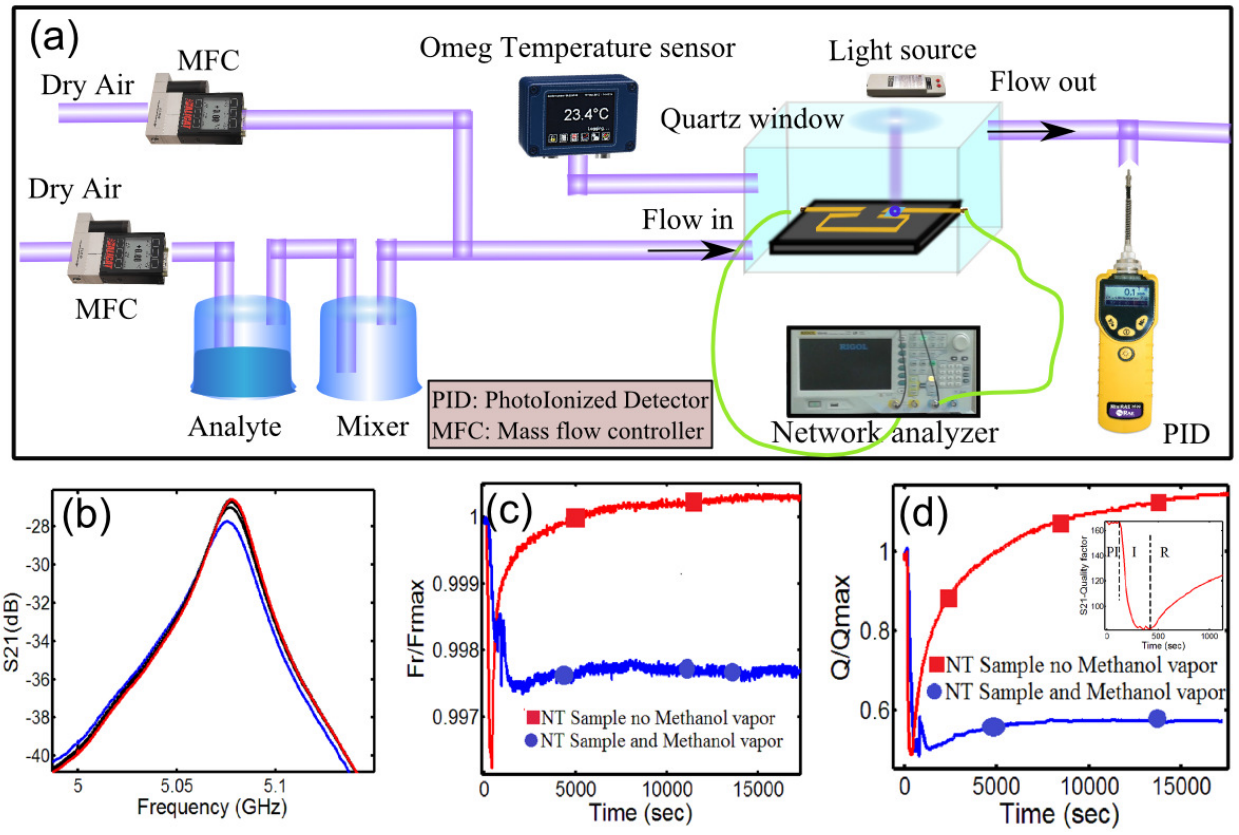

Fig. 3 (a) Schematics of the Experiment setup, (b) S21 profile of the resonator with nanotube and during the illumination time, (c) Normalized resonance frequency variation to the initial resonance frequency of the sensor, (d) Normalized quality factor variation to the initial quality factor of the sensor during the time period of 5 hours; with an inset of *Q* variation with no methanol vapor illustrating a clear transitions between the following phases: prior to illumination (PI) , during illumination (I) and relaxation (R)

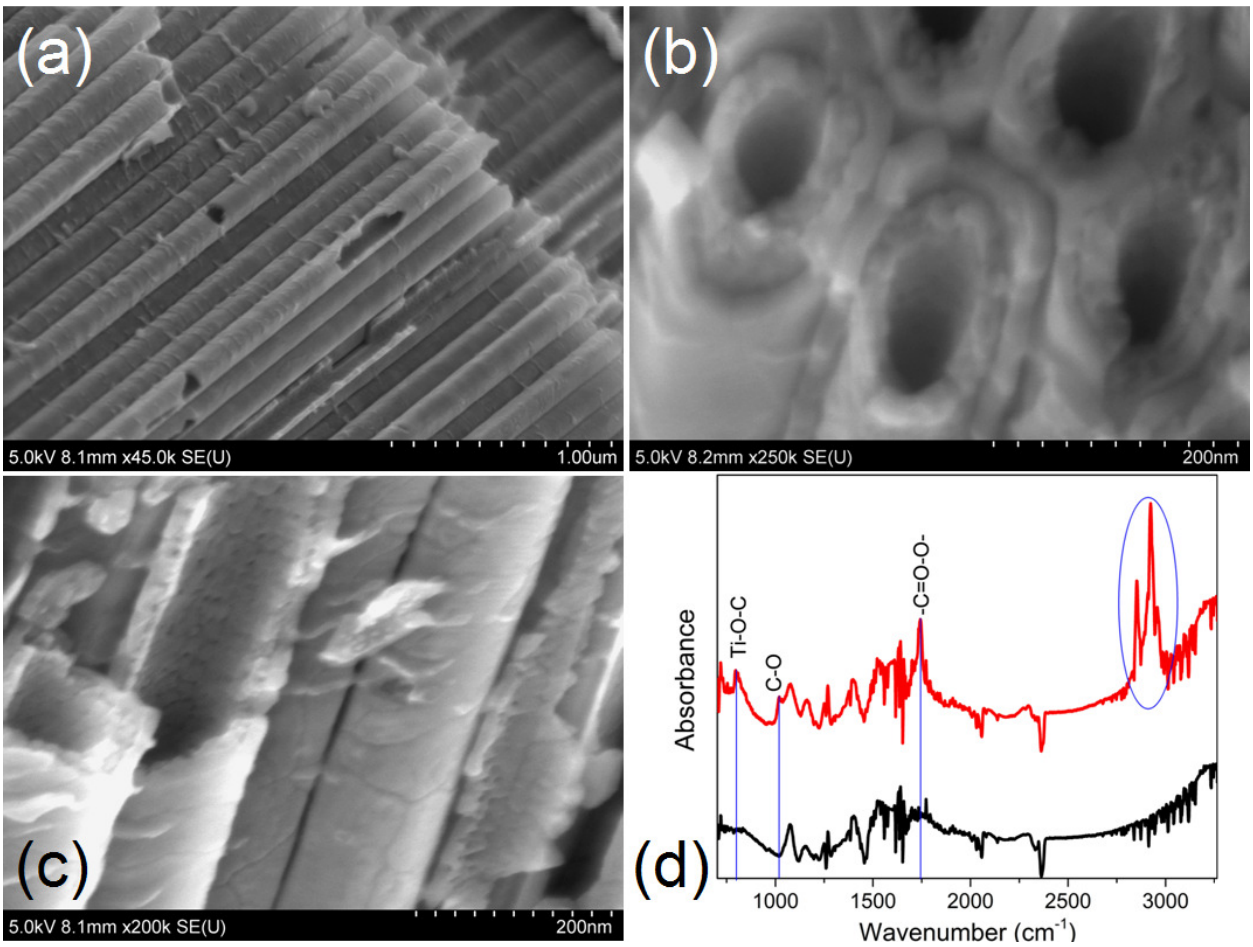

Fig. 4 (a, b, c) FESEM images of the morphology of the TiO_2 nanotubes taken at different angles and magnifications and (d) FTIR spectra of annealed TiO_2 nanotube arrays (black curve) and after exposure to MeOH vapors following the stoppage of illumination (red curve).

Exposing the TiO_2 nanotube membrane to bandgap illumination by ultraviolet photons results in a decrease in both the quality factor (Q) and the resonance frequency (f_0) as shown in Fig. 3. After the illumination is switched off, Q and f_0 recover to their pre-illumination values through a complex multi-exponential decay consisting of time constants in the range of seconds to hours (red curves in Fig. 3, parts c and d). The mechanism of such a long-lived photoconductive response is extensively discussed in a recent publication from our group[24] and in related work.[25, 26] Briefly, ambient oxygen traps free electrons in the TiO_2 nanotubes and the resulting oxide

anionic species chemisorb on to oxygen vacancy sites on the surface of anatase. Trap-filling by photogenerated charges increases the number of bound charges and therefore the effective dielectric constant through the photodielectric effect while also simultaneously producing desorption of the adsorbed oxygen releasing free carriers. The TiO_2 nanotube membranes are ~120 μm thick (Fig. S2 in ESI†) and consist of a well-documented double-walled structure[27-29] as seen in Fig. 4b and Fig. 4c. Fig. 4 parts a, b and c also indicate the outer wall to be relatively smooth while the inner wall has extensive voids and local asperities. The HRTEM electron diffraction pattern in Supporting Information Fig. S3 (in ESI†) confirms the nanotubes to be well-crystallized and composed of the anatase phase. The nanotube membranes thus possess a combination of a high geometric surface area as well as a high local roughness factor, which enables substantial oxygen adsorption on the surface of the membrane in ambient air. This in turn, produces large enough changes in the complex permittivity of the membrane upon UV illumination to produce shifts in f_0 of up to 50 MHz when placed in the coupling gap of the open loop microwave resonator. The orientation of the anatase crystallites in the nanotube walls is also a determinant of the magnitude of the photoresponse since the magnitude of the conductance change following identical UV irradiation is known to be orientation-dependent in TiO_2 single crystals.[30] Spectroscopic microwave measurements using a dielectric probe clearly show a quick and nearly frequency-independent increase in the real permittivity due to illumination and a more gradual decrease after the illumination is turned off (See Fig. S4 in ESI†). The loaded Q-factor in Fig. 3d decreases due to free carrier absorption in the nanotube membrane as well as through alternative dissipative paths in the resonator circuit rendered favorable due to the increase in effective permittivity of the coupling gap. Likewise, the quick increase in the imaginary part of the dielectric constant of the TiO_2 nanotube membrane followed by a much slower return to

equilibrium following the stoppage of illumination is shown in Fig. S5 in ESI†. The long-lived recovery is a signature of thermal trap re-emission processes and is primarily due to the paucity of recombination pathways for free and trapped carriers.

Methanol vapors were introduced into the chamber containing the resonator after the illumination was switched off and the recovery of Q and f_0 to their equilibrium values had commenced. This point in time is marked by the appearance of a transient spike in the temporal plots of both Q and f_0. The adsorption of methanol (by reaction with and/or replacement of chemisorbed oxygen) on the surface of the nanotubes arrests the recovery process and results in a plateauing of the Q and f_0 values close to their illumination values and far away from equilibrium. The drastic change in the resonator response upon the introduction of methanol may be explained on the basis of its hole scavenging action. In the infrared (IR) spectra shown in Fig. 4d, the differences between the IR absorption of the bare membrane and that of the illuminated, methanol exposed membrane are highlighted. The methanol exposed membranes show additional bands at ~798 cm^{-1} and ~1750 cm^{-1} assigned to stretching vibrations of Ti-O-C bonds and ester linkages respectively.[31-33] When combined with the additional C-H stretching bands between 2800 cm^{-1} and 3000 cm^{-1}, the picture that emerges is one of the selective formation of methyl formate by the photocatalytic oxidation of methanol on TiO_2 which is known to involve hole transfer to surface adsorbed methoxy species.[34-36] However, a unique and hitherto unexplored aspect in the present study is that UV illumination of TiO_2 nanotube membranes, and methanol exposure and adsorption do not occur simultaneously. Therefore the methanol in either vapor form or in adsorbed form, does not directly experience the UV photons. Rather, the methanol vapors encounter TiO_2 *after* the stoppage of illumination while it is relaxing back to equilibrium. Adsorbed methanol scavenges reactive trapped holes highly

efficiently and removes the recombination pathway for free and trapped electrons. Consequently, Q and f_0 are unable to recover to their pre-illumination values during the timescale of the experiment.

To compare the effect of different VOC vapors, methanol (MeOH), ethanol (EtOH) and 2-propanol (2-PrOH) were used and their effects on the sensor response were studied by monitoring the resonance frequency and quality factor variation of the sensor in the time domain. In Fig. 5, parts a and b, the kink(s) in the Q and f_0 curves represent the point in time at which the alcohol vapors are introduced into the test chamber. MeOH arrests the recovery in the Q and f_0 curves following the stoppage of illumination and produces a plateauing of the curves far away from equilibrium in contrast to EtOH and 2-PrOH, which have weaker effects on the recovery curves. These results can be understood by considering the adsorption mechanisms and the structure of the alcohols. Aliphatic alcohols adsorb on to TiO_2 surfaces through either molecular adsorption or dissociative chemisorption.[37] However oxygen is adsorbed on the surface of oxygen-deficient polycrystalline anatase nanotubes leaving little room for molecular adsorption.[38] Therefore the alcohols introduced into the test chamber react with adsorbed oxygen on the anatase surface to form adsorbed alkoxy and hydroxyl ions according to the reaction $ROH_g + O^-_{ads} \rightarrow [RO]^-_{ads} + OH^-_{ads}$.[39, 40] Adsorbed oxygen traps electrons and its removal due to the dissociative chemisorption reaction liberates these carriers. Furthermore, recent studies have shown that it is the adsorbed alkoxy rather than the molecularly adsorbed alcohol which is the efficient hole scavenger in alcohols on TiO_2.[36, 41] Consequently, in the case of both MeOH and EtOH, the recovery of Q and f_0 to their equilibrium values is momentarily interrupted immediately following the introduction of alcohol vapors while this effect is much weaker for 2-PrOH. This is understood by considering that the molecular coverage of 2-PrOH, a secondary

alcohol, on anatase TiO_2 and the resulting yield of isopropoxide in temperature programmed desorption experiments is known to be substantially smaller than that of primary alcohols due to steric factors.[37]

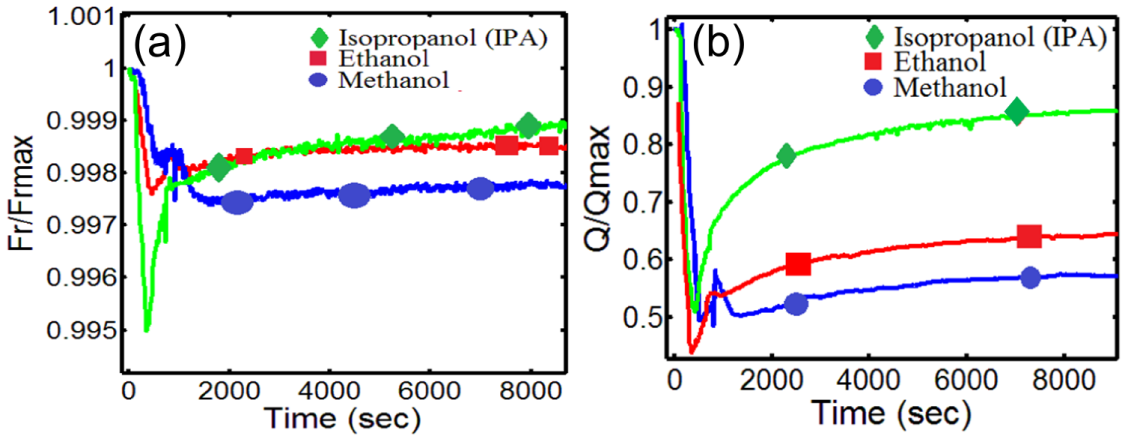

Fig. 5 (a) Resonance frequency variation versus time for 10000 ppm of 2-PrOH (green), EtOH (red) and MeOH (blue) vapors, which are injected 5 minutes after the stoppage of illumination and (b) Quality factor of the resonator sensor versus time for the same vapors.

TiO_2 nanotube arrays have previously been demonstrated to be excellent platforms for the resistive sensing of H_2, CO, NO_2, NH_3, acetone, methane and various alcohols in the vapor phase.[39, 40, 42-49] However, these resistive gas sensors do not exhibit selectivity in their sensing action because all reducing gases and adsorbing molecules which react with adsorbed oxygen reduce the film resistivity by liberating trapped electrons. On the other hand, the divergent recovery levels and time-constants of Q and f_0 for the microwave sensing of the same concentrations of different alcohols demonstrated in Fig. 3 and Fig. 5 provide a fingerprint to obtain selectivity. We have previously shown that the recovery curves of Q and f_0 for UV illuminated TiO_2 nanotube membranes follow tri-exponential decays with a short-lived component in the range of 120-220 s, a slower lifetime in the range of 1000-3000 s and a very slow component with lifetimes extending from 6 hours to several days.[24] In Fig. 3, in the

presence of methanol vapors, both the fastest and slowest components in the recovery curve disappear and only the component with a lifetime of 1000-3000 s is retained, albeit in attenuated form. Exposure to ethanol and 2-propanol vapors causes only the slowest component to vanish (Fig. 5). These contrasting behaviors offer insights into the mechanism of trap-mediated alcohol sensing in photoexcited titania nanotube array membranes. The longest lifetime component occurring at timescales of hours to days is due to the recombination of trapped electrons with trapped holes,[50] and disappears completely due to the scavenging action of alcohols on trapped holes. However the fastest component (120-220 s), which we surmise to be determined by adsorption/re-adsorption kinetics of oxygen on the surface of TiO_2 nanotubes, is quenched only for methanol exposed membranes since only methanol has a diffusivity and surface reactivity strong enough to displace the oxygen completely. Fig. 6 shows the effect of methanol concentration on the microwave response of the sensors. From 400 ppm up to 5000 ppm, exposure of the TiO_2 nanotube arrays to methanol produces distinguishable changes in the temporal microwave response of the resonator. At a MeOH concentration of 10000 ppm, the sensor response is saturated and the recovery curve is arrested. The dynamic range of sensing demonstrated here is comparable to, or superior to recent results from resistive alcohol sensors based on nanostructured TiO_2 and ZnO.[51, 52] Furthermore, the detection of alcohol vapor concentrations below 400 ppm is limited not by the response of the nanotube membrane-mounted resonator but by the ability of the home-built flow setup shown in Fig. 3a to reliably produce air-alcohol mixtures with alcohol concentrations lower than 400 ppm. In Section S2 in ESI†, we show how a number of additional electrical parameters can be extracted for each measurement, which in turn can be used to generate quantitative measures for analyte selectivity.

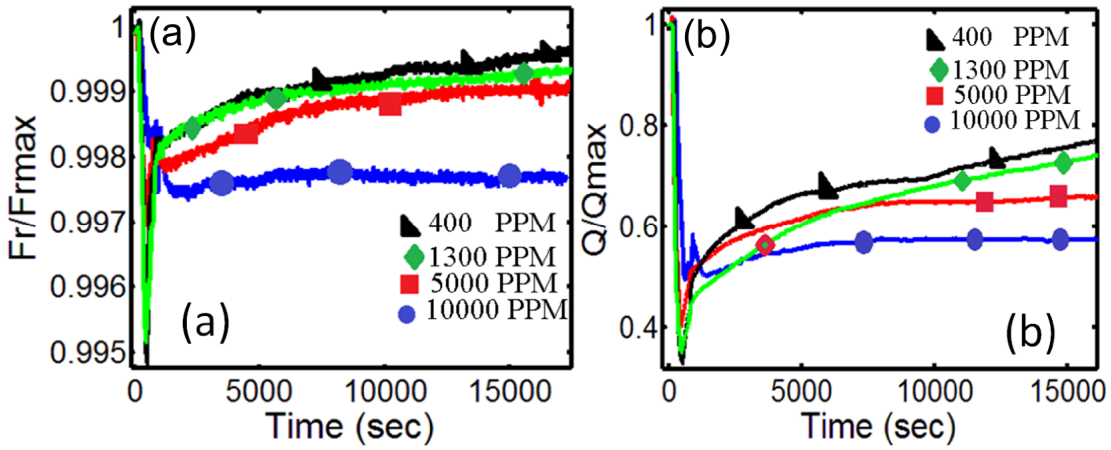

Fig. 6 (a) Resonant frequency and (b) Quality factor response of the nanotube membrane assisted microwave resonator as a function of time for different concentrations of methanol vapor.

The persistent photoconductivity of TiO_2 nanotube arrays and the decreasing costs of violet and ultraviolet LEDs are particularly useful for the sensing modality proposed, since a high-Q membrane-integrated resonator sensor would respond with a sharp change in its f_0 and Q to alcohol vapors introduced any time during a period of hours to days following illumination (charging of the resonator so to speak). The detection of the VOC vapors would provide the signal for re-charging of the sensor. Another useful feature of the proposed sensor configuration is its reusability. The combination of moderate thermal cycling (to desorb adsorbates) followed by an oxygen plasma or UV-ozone treatment (to remove any pyrolyzed organics on the surface) provides a facile means to regenerate the TiO_2 nanotube membrane for sensing.

Very few methods exist to engineer selectivity in the gas sensing action of wide bandgap semiconductors. Even when some selectivity is obtained, the reasons for the behavior are provided *ex post facto* lending no predictive insights.[53] Yet another frontier in sensing consists of the detection of small molecules which have very few binding sites and wherein the binding event itself changes the possibilities of recognition by traditional molecular receptors. In

comparison, the technique we demonstrate in this study allows for the design of selectivity in microwave-based and wide bandgap semiconductor nanostructure-based sensing of small molecules by leveraging the specific interactions of the molecule with the oxide surface, thus producing predictable changes in the conductive and photoconductive microwave response. These interactions include, but are not limited to, electron and hole scavenging effects of adsorbates, electron density donation and acceptance by adsorbates with strong interface dipoles, strong admixture of the molecular orbitals of π-conjugated adsorbates with the semiconductor surface states, and combinations thereof. As a proof of concept, we show how the hole scavenging effect of alcohols on titania can be used to detect short chain aliphatic alcohols as well as distinguish between them.

Acknowledgements

This work was made possible by direct and indirect funding support from NSERC, CFI, Alberta SEGP, CMC Microsystems and NRC-NINT. M. D. would like to acknowledge the Canada Research Chair Program. S.F. thanks Alberta Innovates - Technology Futures for scholarship funding she held during a portion of the period in which this research was conducted.

REFERENCES

1. R. A. Potyrailo and W. G. Morris, *Analytical Chemistry*, 2007, 79, 45-51.
2. M. S. Boybay and O. M. Ramahi, *Instrumentation and Measurement, IEEE Transactions on*, 2012, 61, 3039-3046.
3. L. Chieh-Sen and Y. Chin-Lung, *Sensors Journal, IEEE*, 2014, 14, 695-700.
4. O. Korostynska, A. Mason and A. Al-Shamma'a, *Sensor Review*, 2014, 34, 182-191.
5. M. H. Zarifi, A. Sohrabi, P. M. Shaibani, M. Daneshmand and T. Thundat, *Sensors Journal, IEEE*, 2015, 15, 248-254.
6. M. H. Zarifi, M. Rahimi, M. Daneshmand and T. Thundat, *Sensors and Actuators B: Chemical*, 2016, 224, 632-639.
7. H. Caglayan, S. Cakmakyapan, S. A. Addae, M. A. Pinard, D. Caliskan, K. Aslan and E. Ozbay, *Applied Physics Letters*, 2010, 97.

8. M. Navarro-Cia, M. Aznabet, M. Beruete, F. Falcone, O. El Mrabet, M. Sorolla and M. Essaaidi, *Applied Physics Letters*, 2010, 96.
9. V. Rawat, S. Dhobale and S. N. Kale, *Journal of Applied Physics*, 2014, 116, 164106.
10. M. Schueler, C. Mandel, M. Puentes and R. Jakoby, *Microwave Magazine, IEEE*, 2012, 13, 57-68.
11. M. Ortoneda-Pedrola, O. Korostynska, A. Mason and A. I. Al-Shamma'a, *Journal of Physics: Conference Series*, 2013, 450, 012016.
12. A. A. Abduljabar, A. Porch and D. A. Barrow, 2014.
13. M. Löhndorf, U. Schlecht, T. M. A. Gronewold, A. Malavé and M. Tewes, *Applied Physics Letters*, 2005, 87, 243902.
14. D. Popovic, L. McCartney, C. Beasley, M. Lazebnik, M. Okoniewski, S. C. Hagness and J. H. Booske, *Microwave Theory and Techniques, IEEE Transactions on*, 2005, 53, 1713-1722.
15. S. Clerjon and J. L. Damez, *Measurement Science and Technology*, 2007, 18, 1038.
16. K. Prashanthi, A. Phani and T. Thundat, *Nano Lett.*, 2015, DOI: 10.1021/acs.nanolett.5b02557.
17. R. D. Yang, T. Gredig, C. N. Colesniuc, J. Park, I. K. Schuller, W. C. Trogler and A. C. Kummel, *Applied Physics Letters*, 2007, 90, 263506.
18. J. Li, S. Pud, M. Petrychuk, A. Offenhausser and S. Vitusevich, *Nano Lett.*, 2014, 14, 3504-3509.
19. K. Bayat, J. Choy, M. F. Baroughi, S. Meesala and M. Loncar, *Nano Lett.*, 2014, 14, 1208-1213.
20. H. Clevenson, M. E. Trusheim, C. Teale, T. Schroder, D. Braje and D. Englund, *Nature Physics*, 2015, 11, 393-397.
21. C. Soci, A. Zhang, B. Xiang, S. A. Dayeh, D. P. R. Aplin, J. Park, X. Y. Bao, Y. H. Lo and D. Wang, *Nano Lett.*, 2007, 7, 1003-1009.
22. G. Konstantatos, L. Levina, A. Fischer and E. H. Sargent, *Nano Lett.*, 2008, 8, 1446-1450.
23. A. Mohammadpour, P. Kar, B. D. Wiltshire, A. M. Askar and K. Shankar, *Current Nanoscience*, 2015, 11, 593-614.
24. M. H. Zarifi, A. Mohammadpour, S. Farsinezhad, B. D. Wiltshire, M. Nosrati, A. M. Askar, M. Daneshmand and K. Shankar, *The Journal of Physical Chemistry C*, 2015, DOI: 10.1021/acs.jpcc.5b01066.
25. S. Wendt, P. T. Sprunger, E. Lira, G. K. H. Madsen, Z. Li, J. Ø. Hansen, J. Matthiesen, A. Blekinge-Rasmussen, E. Lægsgaard, B. Hammer and F. Besenbacher, *Science*, 2008, 320, 1755-1759.
26. G. H. Liu, N. Hoivik, X. M. Wang, S. S. Lu, K. Y. Wang and H. Jakobsen, *Electrochim. Acta*, 2013, 93, 80-86.
27. S. P. Albu, A. Ghicov, S. Aldabergenova, P. Drechsel, D. LeClere, G. E. Thompson, J. M. Macak and P. Schmuki, *Advanced Materials*, 2008, 20, 4135-4139.
28. Y. Ji, K.-C. Lin, H. Zheng, J.-j. Zhu and A. C. S. Samia, *Electrochemistry Communications*, 2011, 13, 1013-1015.
29. X. Zhang, F. Han, B. Shi, S. Farsinezhad, G. P. Dechaine and K. Shankar, *Angewandte Chemie*, 2012, 124, 12904-12907.
30. J. Chin, S. Scierka, T. Kim and A. Forster, 2003.

31. M. J. Beliatis, K. K. Gandhi, L. J. Rozanski, R. Rhodes, L. McCafferty, M. R. Alenezi, A. S. Alshammari, C. A. Mills, K. D. G. I. Jayawardena, S. J. Henley and S. R. P. Silva, *Advanced Materials*, 2014, 26, 2078-2083.
32. B. Qiu, Y. Zhou, Y. Ma, X. Yang, W. Sheng, M. Xing and J. Zhang, *Sci. Rep.*, 2015, 5.
33. S. Sakthivel and H. Kisch, *Angewandte Chemie International Edition*, 2003, 42, 4908-4911.
34. H. Kominami, H. Sugahara and K. Hashimoto, *Catalysis Communications*, 2010, 11, 426-429.
35. Q. Guo, C. Xu, W. Yang, Z. Ren, Z. Ma, D. Dai, T. K. Minton and X. Yang, *The Journal of Physical Chemistry C*, 2013, 117, 5293-5300.
36. K. R. Phillips, S. C. Jensen, M. Baron, S.-C. Li and C. M. Friend, *Journal of the American Chemical Society*, 2013, 135, 574-577.
37. K. S. Kim, M. A. Barteau and W. E. Farneth, *Langmuir*, 1988, 4, 533-543.
38. S. Funk, B. Hokkanen, U. Burghaus, A. Ghicov and P. Schmuki, *Nano Lett.*, 2007, 7, 1091-1094.
39. A. Hazra, K. Dutta, B. Bhowmik, P. P. Chattopadhyay and P. Bhattacharyya, *Applied Physics Letters*, 2014, 105.
40. A. Hazra, B. Bhowmik, K. Dutta, P. P. Chattopadhyay and P. Bhattacharyya, *ACS Applied Materials & Interfaces*, 2015, 7, 9336-9348.
41. M. Shen and M. A. Henderson, *The Journal of Physical Chemistry Letters*, 2011, 2, 2707-2710.
42. B. M. Rao and S. C. Roy, *Rsc Advances*, 2014, 4, 49108-49114.
43. S. Yoriya, H. E. Prakasam, O. K. Varghese, K. Shankar, M. Paulose, G. K. Mor, T. J. Latempa and C. A. Grimes, *Sensor Letters*, 2006, 4, 334-339.
44. M.-H. Seo, M. Yuasa, T. Kida, J.-S. Huh, K. Shimanoe and N. Yamazoe, *Sensors and Actuators B-Chemical*, 2009, 137, 513-520.
45. E. Sennik, Z. Colak, N. Kilinc and Z. Z. Ozturk, *International Journal of Hydrogen Energy*, 2010, 35, 4420-4427.
46. V. Galstyan, E. Comini, G. Faglia, A. Vomiero, L. Borgese, E. Bontempi and G. Sberveglieri, *Nanotechnology*, 2012, 23.
47. V. Galstyan, E. Comini, G. Faglia and G. Sberveglieri, *Sensors*, 2013, 13, 14813-14838.
48. P. M. Perillo and D. F. Rodríguez, *Sensors and Actuators B: Chemical*, 2012, 171–172, 639-643.
49. H. G. Liu, D. Y. Ding, C. Q. Ning and Z. H. Li, *Nanotechnology*, 2012, 23.
50. S. C. Ke, T. C. Wang, M. S. Wong and N. O. Gopal, *Journal of Physical Chemistry B*, 2006, 110, 11628-11634.
51. N. Banerjee, S. Roy, C. K. Sarkar and P. Bhattacharyya, *Sensors Journal, IEEE*, 2013, 13, 1669-1676.
52. A. Hazra, K. Dutta, B. Bhowmik and P. Bhattacharyya, *Sensors Journal, IEEE*, 2015, 15, 408-416.
53. S. A. Geetha, M. Abhishek, V. D. Albert, P. O. Vladimir, A. B. Kris, A. S. Norman and V. M. Rao, *Nanotechnology*, 2012, 23, 175501.